THE INHIBITING EFFECT OF NO ADDITION ON DIMETHYL ETHER HIGH-PRESSURE OXIDATION

Lorena Marrodán, Álvaro J. Arnal, Ángela Millera, Rafael. Bilbao, María U. Alzueta*

Aragón Institute of Engineering Research (I3A). Department of Chemical and Environmental Engineering. University of Zaragoza. C/ Mariano Esquillor, s/n. 50018 Zaragoza. Spain

*uxue@unizar.es

ABSTRACT

The high-pressure dimethyl ether (DME, CH_3OCH_3) oxidation has been investigated in a plug flow reactor in the 450-1050 K temperature range. Different pressures (20, 40 and 60 bar), air excess ratios (λ=0.7, 1 and 35), and the absence/presence of NO have been tested, for the first time under these conditions. An early reactivity of DME and a negative temperature coefficient (NTC) zone have been observed under the studied conditions, although under very oxidizing conditions (λ=35), NTC zone is almost imperceptible because DME is completely consumed at lower temperatures. A chemical kinetic mechanism has been used to describe the DME high-pressure oxidation, with a good agreement with the experimental trends observed. In general, modeling calculations with the present mechanism have been successfully compared with experimental data from literature. The presence of NO has an inhibiting effect on DME high-pressure consumption at low-temperatures because of: (i) the competition between $CH_3OCH_2 + O_2 \rightleftharpoons CH_3OCH_2O_2$ and $CH_3OCH_2 + NO_2 \rightleftharpoons CH_3OCH_2O + NO$ reactions, and (ii) the participation of NO in $CH_3OCH_2O_2 + NO \rightleftharpoons CH_3OCH_2O + NO_2$ reaction, preventing $CH_3OCH_2O_2$ radicals continue reacting through a complex mechanism, which includes a second O_2 addition and several isomerizations and decompositions, during which highly reactive OH radicals are generated. Consequently, NO and NO_2 are interchanged in a cycle but never consumed.

Keywords: dimethyl ether; oxidation; high-pressure; nitrogen oxides; modeling

1. Introduction

Current problems derived from the intense use of fossil fuels make the search for more environmentally friendly fuels and new combustion techniques urgent. The second-generation biofuels, derived from biomass wastes, are considered to be clean and CO_2 neutral. Dimethyl ether (DME, CH_3OCH_3), due to its high cetane number (>55), almost immediate vaporization as sprayed into the cylinder, rich oxygen content (around 35 % by mass), no C-C bonds, and lower autoignition temperature compared to diesel fuel, is considered as a good alternative [1]. It can be a substitute for Liquefied Petroleum Gas (LPG), diesel fuel and Liquefied Natural Gas (LNG) [2, 3]. Therefore, DME conversion has been subject of numerous studies carried out in different types of reactors and conditions. For example, Rodriguez et al. [4], in their study of low-temperature oxidation of DME, performed a great review of some of the most recent experimental studies, 34 different works performed in jet-stirred reactors, flow tubes, shock tubes, rapid compression machines, burners and spherical bombs.

Diesel engines involve conditions where interactions between fuel components and nitrogen oxides are possible. For example, the recycling of some of the exhaust gas back into the engine system, commonly known as exhaust gas recirculation (EGR), is a strategy of limiting the production of pollutants by diluting the reactants with exhaust gas, allowing operation under fuel-lean conditions and lower temperatures. New combustion techniques, such as low temperature combustion (LTC), homogeneous charge compression ignition (HCCI) and premixed charge compression ignition (PCCI), also include EGR systems to achieve low emissions of NO_x and soot [5, 6]. Thereby, it is interesting to analyze the role of the NO formed during the fuel combustion and once it has been recycled, because it may have a significant impact on autoignition.

Numerous previous studies have analyzed the interaction between NO and different fuels such as hydrocarbons [7-13] or alcohols [14, 15] showing that, depending on the combustion conditions, the impact of NO can be completely different. At high temperatures and fuel-rich conditions, NO may be reduced to N_2 and HCN by reacting with hydrocarbon radicals in reburn-type reactions (e.g. [16]); whereas at low to intermediate temperatures, the presence of

NO may promote the oxidation of the fuel (e.g. [12]), but also the oxidation of NO to NO_2 may be promoted by the fuel in a mutually sensitized oxidation process, as reported by Dagaut and Nicolle during the oxidation of methane in the presence of NO [10]. However, the presence of NO can also have inhibiting effects on fuel conversion. Moréac et al. [8], in a n-heptane jet-stirred oxidation work at 10 atm, reported that the effects of the NO presence vary with temperature; that is, at low temperatures NO may have an inhibiting effect, whereas at temperatures higher than 675 K, NO may accelerate the reactivity. The addition of NO may inhibit the reaction to the point of extinction in the negative temperature coefficient (NTC) region, that is of primary importance for the autoignition, due to the NO+OH=HONO reaction; but at higher temperatures, the HO_2 concentration is increased and it allows the regeneration of reactive OH radicals through $NO+HO_2=NO_2+OH$. Moreover, Anderlohr et al. [13] suggested a mechanism to explain this inhibiting effect of NO in the NTC zone of n-heptane oxidation. The competition between $RO_2+NO=RO+NO_2$ and the second O_2 addition could be the main cause for the inhibiting effect at temperatures higher than 650 K. Below this temperature, the NO+OH=HONO reaction seems to be the inhibiting one.

Despite the large number of studies concerning the interaction of fuel components with NO or the DME oxidation, to our knowledge, only a previous work of our group focuses on the direct interaction of DME and NO in an atmospheric plug flow reactor [17]. Other study [18], also from our group and under atmospheric conditions, analyzes the effect of the addition of NO to mixtures of DME and acetylene, as a soot precursor. Besides, since engine efficiency is increased by working under high-pressure conditions, reliable experimental data for validation of the kinetic models at these conditions become very relevant.

In this scenario, the present work aims to analyze the influence of the presence of NO on the high-pressure oxidation of DME, which, to our knowledge, has not been considered earlier. For this analysis, it is also interesting to first characterize the DME oxidation under high-pressure conditions. Therefore, an experimental and kinetic study of DME high-pressure (20, 40 and 60 bar) oxidation has been carried out in the 450-1050 K temperature range. In addition to

stoichiometric conditions, oxidation data have been collected under strongly oxidizing and slightly reducing conditions, both in the absence and presence of NO (500 ppm).

2. Experimental section

The experimental setup used to perform the high-pressure DME oxidation experiments, in the absence and presence of NO, has been previously described in detail [19], so only a description of the main features is provided here. Reactants, DME (approximately 700 ppm), NO (approximately 500 ppm) and O_2, and N_2 as carrier gas, were supplied from gas cylinders through mass flow controllers with an uncertainty in the flow rate measurements of approximately 0.5%. The oxygen required to carry out each oxidation experiment is determined by the air excess ratio (λ, defined as the inlet oxygen divided by stoichiometric oxygen). Table 1 contains the conditions for the different experiments.

Table 1. Matrix of experimental conditions. Experiments were conducted in the 450-1050 K temperature range. The balance is closed with N_2.

Set	DME [ppm]	NO [ppm]	P [bar]	λ	t_r [s]	Flow rate [L(STP)/min]
1	700	-	20	0.7	5220/T	1
2	698	-	20	1	5220/T	1
3	700	-	20	35	5220/T	1
4	692	-	40	0.7	10440/T	1
5	695	-	40	1	10440/T	1
6	700	-	40	35	10440/T	1
7	704	-	60	0.7	15660/T	1
8	702	-	60	1	15660/T	1
9	700	-	60	35	15660/T	1
10	732	-	40	0.7	5220/T	2
11	698	-	40	1	5220/T	2
12	700	-	40	35	5220/T	2
13	710	518	20	0.7	5220/T	1
14	700	498	20	1	5220/T	1
15	700	490	20	35	5220/T	1
16	702	502	40	0.7	10440/T	1
17	695	485	40	1	10440/T	1
18	723	497	40	35	10440/T	1
19	710	479	60	0.7	15660/T	1
20	703	515	60	1	15660/T	1
21	700	487	60	35	15660/T	1

The reactant gases were premixed before entering the reactor, which consists of a tubular quartz tube (inner diameter of 6 mm and 1500 mm in length) designed to approximate plug flow [20].

The reactor is enclosed in a stainless-steel pressure shell and it, in turn, in an electrically heated oven. The temperature is monitored by K-thermocouples placed between the quartz reactor and the steel shell. The longitudinal temperature profiles were experimentally determined in N_2 atmosphere, obtaining an isothermal (±10 K) reaction zone of 56 cm. An example of the temperature profiles inside the reactor for a flow rate of 1 L(STP)/min, and 20, 40 and 60 bar can be found in the Supplementary Material (Figures S1-S3). Moreover, an excel spreadsheet with all the temperature-distance profiles is provided as Supplementary Material. Two different gas flow rates were tested (1 and 2 L(STP)/min) resulting in different temperature-dependent gas residence times (t_r) according to the working pressure. In the case of the higher gas flow rate studied in this work, 2 L(STP)/min, the temperature profiles were also checked, and they were very similar to those determined for 1 L(STP)/min. In all the cases, nitrogen was used to balance.

The gases leaving the reactor were on-line analyzed by a micro-gas chromatograph (Agilent 3000A) equipped with Thermal Conductivity Detectors (TCD), an ATI Mattson Fourier Transform Infrared (FTIR), and a continuous IR NO analyzer (URAS26 ABB). The uncertainty of the measurements is estimated as ±5%, except for the FTIR spectrometer, which is estimated ±10%.

3. Chemical kinetic model

The first detailed gas-phase chemical kinetic mechanism, used for chemistry description and analysis of the present experimental results, was taken from a study of the atmospheric oxidation of acetylene-dimethyl ether mixtures, in the absence and presence of NO, developed by our research group [18], to which modifications have been made in this work as described below. The basis of this first mechanism consists of reactions to describe C_1-C_2 and NO interactions and it was initially proposed by Glarborg et al. [16] and progressively updated (e.g. [21]). This mechanism [18] also includes reactions to describe acetylene [22], ethanol [14], glyoxal [23] and DME [17] conversion. When the mechanism of reference [18] was used to simulate the present high-pressure experimental results, the mechanism was not able to describe properly the characteristic NTC behavior of DME occurring at low temperature and high

pressure. Therefore, improvements of the mechanism from reference [18], which was validated at atmospheric pressure, are required.

This mechanism has been updated and modified to consider the high-pressure experimental conditions of this work [20, 24-27]. The subset for DME has also been revised according to DME kinetic mechanisms from literature, Zhao's et al. [28] and Burke's et al. mechanisms [29], validated against a wide range of experimental data. Burke et al. [29] assessed the pressure dependencies of the reactions involved in the low-temperature oxidation pathways for DME. Under the experimental conditions studied in that work, the prediction of the ignition delay times was found to be particularly sensitive to the decomposition of the CH_3OCH_2 radical ($CH_3OCH_2=CH_3+CH_2O$). Therefore, only the pressure dependency of this reaction was updated through a more sophisticated treatment by Burke et al. [29]. However, under the present conditions, results are sensitive to the isomerization of alkyl-peroxyl radicals to form hydroperoxyl alkyl radicals ($CH_3OCH_2O_2=CH_2OCH_2O_2H$). The impact of such reaction is later discussed.

The reactions for DME, that have been modified or added compared to Alzueta et al. reaction subset [17], are specified in Table 2.

As previously mentioned, the variety of experimental and modeling studies on DME conversion is very large. The performance of some of the most recent mechanisms [4, 28, 30, 31] has been compared against the present high-pressure experimental data. The comparisons can be found in Figures S4-S6 in Supplementary Material. In general, those mechanisms are able to reproduce the experimental trends. An interesting issue when comparing the different mechanisms is the different reaction pathways considered. An aspect of interest is related to the presence and reactions of formic acid (HCOOH). Our experimental results evidence the formation of HCOOH from DME and, actually, HCOOH has a significant role under our conditions. The mechanism proposed by Rodriguez et al. [4] does not include HCOOH as intermediate, and although other mechanisms (for example, Zhao et al.'s mechanism [28]) suggested some reactions involving formic acid, in the present work, we have included the more recent subset

for the oxidation of formic acid based on ab initio calculations proposed by Marshall and Glarborg [32].

The present mechanism also includes reaction subsets for methyl formate [19], dimethoxymethane [33] and ethanol [34], validated in previous works under similar experimental conditions, even though they are not especially relevant to this study.

In the case of reactions involving NO and NO_2, no major modifications have been made with respect to previous works from our group under similar conditions (e.g. [34]). The basis mechanism from Glarborg et al. [16] contains reactions to describe the interactions between C_1-C_2 and NO. These reactions have been updated according to more recent works involving NO_x, which were developed and validated for high-pressure conditions [20, 26]. Reactions for coupling both DME and NO_x subsets, such as $CH_3OCH_2+NO_2=CH_3OCH_2O+NO$ or $CH_3OCH_2O_2+NO=CH_3OCH_2O+NO_2$, were already considered in the initial DME reaction subset [17]. Only one modification was made in our previous study [34], we included reaction (R_1) to reproduce the highly expected interaction between CH_3 radicals and NO_2 under high-pressure conditions.

$$CH_3ONO \rightleftharpoons CH_3 + NO_2 \qquad (R_1)$$

Table 2. Reactions for DME modified or added compared to Alzueta et al.'s work [17]; units: cm^3, mol, s and cal.

Reaction		A	n	E_a	source
$CH_3OCH_3(+M)=CH_3+CH_3O(+M)$	(high-pressure)	4.37×10^{21}	-1.57	83842	[28]
	(low-pressure)	1.13×10^{62}	-12.19	94882	
$CH_3OCH_3+OH=CH_3OCH_2+H_2O$		6.71×10^{6}	2.00	-629.88	[28]
$CH_3OCH_3+HO_2=CH_3OCH_2+H_2O_2$		2.00×10^{13}	0.00	16500	[28]
$CH_3OCH_3+CH_3=CH_3OCH_2+CH_4$		2.68×10^{1}	3.78	9631.3	[28]
$CH_3OCH_3+CH_3O_2=CH_3OCH_2+CH_3O_2H$		1.27×10^{-3}	4.64	10556	[29]
$CH_3OCH_3+CH_3OCH_2O_2=CH_3OCH_2+CH_3OCH_2O_2H$		5.00×10^{12}	0.00	17690	[29]
$CH_3OCH_3+OCHO=CH_3OCH_2+HOCHO$		1.00×10^{13}	0.00	17690	[29]
$CH_3OCH_2=CH_3+CH_2O$		8.03×10^{12}	0.44	26490	[29]
	(0.001 atm)	7.49×10^{23}	-4.52	25236	
	(0.01 atm)	6.92×10^{28}	-5.73	27494	
	(1 atm)	4.23×10^{29}	-5.61	28898	
	(10 atm)	6.61×10^{27}	-4.71	29735	
	(100 atm)	2.66×10^{29}	-4.94	31785	
$CH_3OCH_2+O_2=CH_3OCH_2O_2$	(0.001 atm)	1.12×10^{18}	-3.37	-4294	[29]
	(0.01 atm)	1.33×10^{21}	-3.95	-2615	
	(1 atm)	1.13×10^{28}	-5.24	4088	

	(2 atm)	3.91×10^{27}	-5.00	4512	
	(10 atm)	2.75×10^{24}	-3.87	4290	
	(20 atm)	2.97×10^{22}	-3.23	3781	
	(50 atm)	5.19×10^{19}	-2.35	2908	
	(100 atm)	5.43×10^{17}	-1.73	2210	
$CH_3OCH_2+O_2=CH_2OCH_2O_2H$	(0.001 atm)	5.08×10^{20}	-4.39	469	[29]
	(0.01 atm)	5.47×10^{23}	-4.96	2183	
	(1 atm)	2.81×10^{28}	-5.63	7848	
	(2 atm)	5.19×10^{27}	-5.33	8144	
	(10 atm)	9.67×10^{24}	-4.40	8417	
	(20 atm)	4.08×10^{23}	-3.90	8494	
	(50 atm)	5.08×10^{21}	-3.30	8585	
	(100 atm)	1.62×10^{20}	-2.80	8619	
$CH_3OCH_2+O_2=CH_2O+CH_2O+OH$	(0.001 atm)	8.01×10^{21}	-3.20	3067	[29]
	(0.01 atm)	1.73×10^{23}	-3.50	4050	
	(1 atm)	2.04×10^{31}	-5.80	11594	
	(2 atm)	5.99×10^{31}	-5.90	12710	
	(10 atm)	9.39×10^{30}	-5.60	14517	
	(20 atm)	1.09×10^{30}	-5.30	15051	
	(50 atm)	3.58×10^{28}	-4.90	15664	
	(100 atm)	2.41×10^{27}	-4.50	16107	
$CH_3OCH_2O=CH_3O+CH_2O$		9.72×10^{15}	-1.10	20640	[28]
$CH_3OCH_2O_2+CH_3OCH_2O_2=O_2+CH_3OCH_2O+CH_3OCH_2O$		1.60×10^{23}	-4.50	0	[28]
$CH_3OCH_2O_2+CH_3OCH_2O_2=O_2+CH_3OCHO+CH_3OCH_2OH$		6.84×10^{22}	-4.50	0	[28]
$CH_3OCH_2O_2=CH_2OCH_2O_2H$	(0.001 atm)	1.94×10^{29}	-6.99	22446	[29]
	(0.01 atm)	4.07×10^{27}	-6.16	21619	
	(1 atm)	2.52×10^{25}	-4.76	22691	
	(2 atm)	5.97×10^{24}	-4.48	22868	
	(10 atm)	4.44×10^{21}	-3.38	22386	
	(20 atm)	4.52×10^{19}	-2.74	21803	
	(50 atm)	5.72×10^{16}	-1.82	20829	
	(100 atm)	3.70×10^{14}	-1.13	20034	
$CH_3OCH_2O_2=CH_2O+CH_2O+OH$	(0.001 atm)	2.06×10^{36}	-8.30	33415	[29]
	(0.01 atm)	2.07×10^{39}	-8.90	35842	
	(1 atm)	1.12×10^{40}	-8.40	39835	
	(2 atm)	9.72×10^{38}	-8.00	39923	
	(10 atm)	6.28×10^{35}	-7.00	39900	
	(20 atm)	1.60×10^{34}	-6.50	39850	
	(50 atm)	8.32×10^{31}	-5.80	39719	
	(100 atm)	1.22×10^{30}	-5.20	39549	
$CH_2OCH_2O_2H=OH+CH_2O+CH_2O$	(0.001 atm)	1.66×10^{23}	-4.53	22243	[29]
	(0.01 atm)	5.30×10^{25}	-4.93	24158	
	(1 atm)	7.81×10^{22}	-3.50	23156	
	(2 atm)	4.98×10^{22}	-3.35	23062	
	(10 atm)	8.46×10^{22}	-3.22	23559	
	(20 atm)	9.09×10^{22}	-3.14	23899	
	(50 atm)	4.59×10^{22}	-2.94	24262	
	(100 atm)	1.40×10^{22}	-2.72	24407	
$CH_2OCH_2O_2H+O_2=>O_2CH_2OCH_2O_2H$	(0.001 atm)	9.42×10^{12}	-1.68	-4998	[29]
	(0.01 atm)	8.16×10^{16}	-2.50	-2753	
	(1 atm)	1.06×10^{22}	-3.30	3389	
	(2 atm)	3.48×10^{20}	-2.79	3131	
	(10 atm)	2.86×10^{16}	-1.48	1873	
	(20 atm)	8.55×10^{14}	-1.01	1312	
	(50 atm)	2.68×10^{13}	-0.54	727	
	(100 atm)	4.87×10^{12}	-0.32	428	
$CH_2OCH_2O_2H+O_2=>HO_2CH_2OCHO+OH$	(0.001 atm)	5.90×10^{20}	-2.88	3234	[29]
	(0.01 atm)	2.06×10^{23}	-3.59	5116	
	(1 atm)	4.45×10^{29}	-5.29	12791	
	(2 atm)	2.44×10^{28}	-4.92	12891	

	(10 atm)	9.42×10^{23}	-3.68	12049	
	(20 atm)	1.04×10^{22}	-3.16	11505	
	(50 atm)	6.95×10^{19}	-2.60	10861	
	(100 atm)	3.96×10^{18}	-2.31	10500	
$O_2CH_2OCH_2O_2H=HO_2CH_2OCHO+OH$	(0.001 atm)	9.05×10^{23}	-4.88	18805	[29]
	(0.01 atm)	6.84×10^{26}	-5.32	22533	
	(1 atm)	5.07×10^{16}	-1.81	21175	
	(2 atm)	2.66×10^{14}	-1.11	20310	
	(10 atm)	1.69×10^{10}	0.18	18604	
	(20 atm)	1.11×10^{09}	0.54	18100	
	(50 atm)	1.07×10^{08}	0.84	17661	
	(100 atm)	3.86×10^{07}	0.98	17467	
$HO_2CH_2OCHO=>OCH_2OCHO+OH$		3.00×10^{16}	0.00	43000	[28]
$CH_2O+OCHO=OCH_2OCHO$		1.25×10^{11}	0.00	11900	[29]
$HOCH_2OCO=HOCH_2O+CO$		2.18×10^{16}	-2.69	17200	[28]
$HOCH_2OCO=CH_2OH+CO_2$		5.31×10^{15}	-2.61	20810	[28]
$HOCH_2O=HCOOH+H$		1.00×10^{14}	0.00	14900	[28]
$CH_2O+OH=HOCH_2O$		4.50×10^{15}	-1.11	0	[28]

Thermochemistry involved in modeling DME conversion has been extensively studied, and significant discrepancies can be found in enthalpy and entropy of formation as well as heat capacities for the different species involved in the conversion of DME. We have done a review of the different thermodynamic values of the literature and Table S1 in the Supplementary Material lists the different thermodynamic properties for those selected species of relevance for DME conversion: CH_3OCH_2, $CH_3OCH_2O_2$ and $CH_2OCH_2O_2H$. In Table S1, thermodynamic data calculated from the mechanism information given by different authors [4, 28-31], together with the theoretical determination by Yamada et al. [35], are shown. As it can be observed, there is a large discrepancy between the values used for the different authors, especially for CH_3OCH_2. Moreover, the values can differ depending on the temperature range used for calculations, low or high temperature range.

The thermodynamic data that we have used for the species involved in DME reaction subset have been taken from Burke et al. [29] to be consistent with the source of the kinetic parameters.

The final mechanism, which involves 138 species and contains 792 reactions, and the thermodynamic data files, both in CHEMKIN format, are provided as Supplementary Material. Numerical calculations were conducted with the plug-flow reactor module of CHEMKIN-PRO

software package [36] and taking into account the temperature profiles experimentally determined.

An example of the relevance of the different modifications done to the mechanism [18] is shown in Figure S7 in Supplementary Material. As it can be observed, the match between experimental results and modeling calculations improves considerably with the modifications in Table 2.

Moreover, modeling calculations obtained with the present mechanism have been compared against several sets of data from literature covering a wide range of experimental devices and conditions (Figures S8-S17 in Supplementary Material). In general, the present mechanism reproduces well the different experimental data from literature.

4. Results and discussion

The main purpose of this work is to analyze the effect of the addition of NO on the high-pressure oxidation of DME. Therefore, before analyzing its effect, the high-pressure oxidation of DME should be well characterized.

4.1 High-pressure DME oxidation in the absence of NO

The influence of the pressure (20, 40 and 60 bar), the oxygen availability (determined by different air excess ratios, λ), and the presence of NO has been evaluated in the 450-1050 K high-pressure DME oxidation.

Figure 1 shows, for a selected experiment (set 10 in Table 1), the evolution with temperature of the reactants (DME and O_2) and main products (CO, CO_2, CH_4, HCOOH, H_2) concentration experimentally obtained. In the 550-750 K temperature range, there is a "plateau" in DME where it remains constant. It corresponds to the negative temperature coefficient (NTC) zone, where DME reactivity is constant or decreases with temperature, and it is also reflected in the concentration profile of the other compounds. It is more pronounced in the oxygen concentration profile, in which two inflection points characterizing the NTC zone can be identified. From now on, we will focus mainly on DME concentration profile to analyze the influence of the different variables.

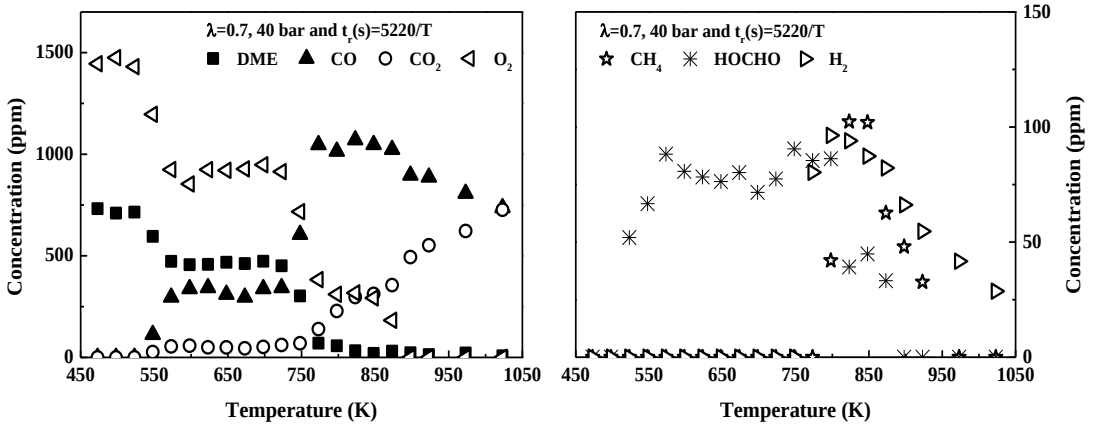

Figure 1. Evolution for DME, O_2, CO, CO_2, CH_4, HCOOH and H_2 concentrations with temperature during the high-pressure (20 bar) oxidation of DME, for the conditions denoted as set 10 in Table 1 (λ=0.7, 2 L(STP)/min, in the absence of NO).

Considering the experimental procedure followed in the current setup, a change in the working pressure while maintaining the total gas flow rate, also implies a change in the gas residence time. That is, for 1 L(STP)/min of total flow rate, the gas residence time is $t_r(s)=261\ P(bar)/T(K)$, which implies that residence time depends on both pressure and temperature. Therefore, we have performed different experiments to try to distinguish between the effect of gas residence time or pressure. To analyze the influence of the pressure, the gas residence time was kept "constant", only as a function of temperature, $t_r(s)=5220/T(K)$, and the pressure was increased from 20 to 40 bar. On the other hand, to analyze the influence of the gas residence time, the pressure was kept constant (40 bar) and the residence time was changed from $t_r(s)=5220/T(K)$ to $t_r(s)=10440/T(K)$. Figure 2 shows the experimental results (symbols) and modeling calculations (lines) obtained in this way for the three different values of lambda analyzed.

As shown in Figure 2, in general, there is a good agreement between experimental results and modeling calculations for DME conversion. In the 550-700 K temperature range, the NTC behavior is observed for all the conditions analyzed, although is less pronounced under very oxidizing (λ=35) conditions because the high oxygen availability causes the DME to be

completely consumed at lower temperatures. This will be discussed later when analyzing the influence of pressure and lambda on DME oxidation. For the same residence time, increasing the pressure from 20 to 40 bar, does not seem to have a big effect on DME conversion for any of the lambda values analyzed. For the same pressure and λ=0.7 and λ=1, the oxidation of DME is favored by increasing the gas residence time, whereas for λ=35 no big changes are noticed. In conclusion, under the operating conditions used in this work, the effect on DME high-pressure oxidation of the residence time is clear and more noticeable than the effect of pressure. In a previous high-pressure oxidation of ethanol under similar conditions to those of this work [34], an analysis of the influence of pressure and residence time was also carried out, but only from a modeling point of view, elucidating that both pressure and residence time had an appreciable impact shifting ethanol conversion to lower temperatures when any of these variables was increased.

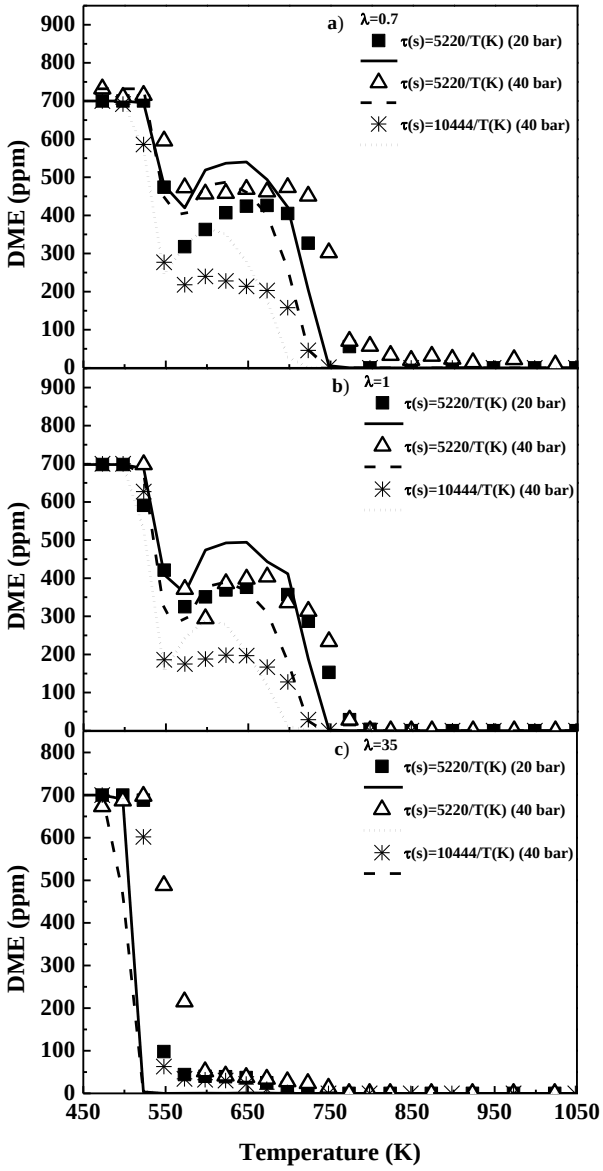

Figure 2. Evaluation of the effect of pressure and gas residence time on the high-pressure (20 or 40 bar) oxidation of DME, for the conditions denoted as (a) sets 1, 10 and 4 in Table 1 for λ=0.7; (b) sets 2, 11 and 5 in Table 1 for λ=1; and (c) sets 3, 12 and 6 in Table 1 for λ=35.

4.2 High-pressure DME oxidation in the presence of NO

The influence of NO presence (500 ppm) on the high-pressure (20, 40 and 60 bar) DME oxidation has been analyzed in the 450-1050 K temperature range, from reducing (λ=0.7) to very oxidizing conditions (λ=35). As it has been explained, the results presented from now on, correspond to the joint effect of pressure and residence time, with a more relevance of the latter.

Furthermore, under the present experimental conditions, it has been observed that NO added to the reactant mixture can be converted to NO_2 before entering the reactor, because of the high-pressure conditions and the presence of O_2, through reaction (R_2).

$$2NO + O_2 \rightleftharpoons 2NO_2 \qquad (R_2)$$

Figure 3 shows the evolution with temperature of theoretical and experimental NO outlet concentrations for the different pressures and values of lambda analyzed. Model reproduces quite well the experimental trends observed although some improvements could be done, in particular at high pressure and high temperature, where the model deviates from experimental results. At present, we are not able to explain the reasons for such discrepancy. Under these conditions, the formation of stable peroxide nitrogenous species may occur, but not easy to be detected experimentally. At temperatures below 650 K, for λ=0.7 and 1, the experimental NO concentration remains in a low value and, at higher temperatures, it starts to increase to reach almost the inlet concentration value in the case of 20 bar and a slightly lower concentration for 40 and 60 bar. Only for λ=35, the experimental NO concentration remains almost constant in very low concentration, less than 50 ppm, in the highest case.

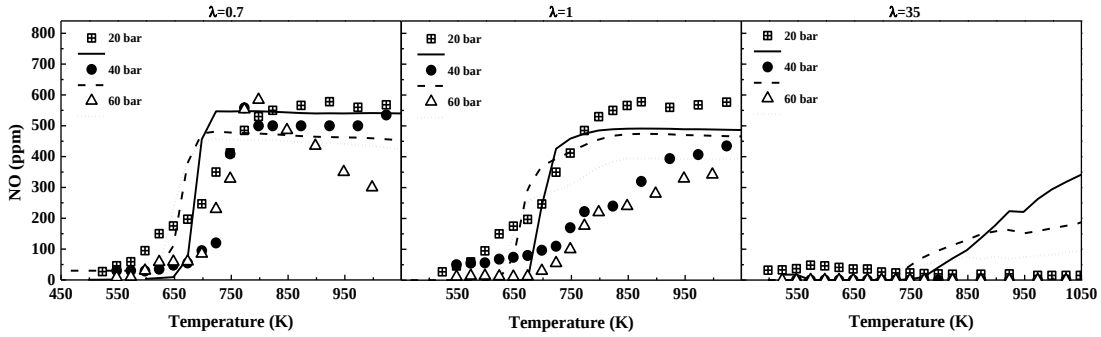

Figure 3. Evolution for NO concentration with temperature during the high-pressure (20, 40 and 60 bar) oxidation of DME, for the conditions denoted as sets 13-21 in Table 1.

In the same way, Figure 4 shows the evolution with temperature of the DME concentration profile for different pressures and values of lambda, in the presence and absence of NO.

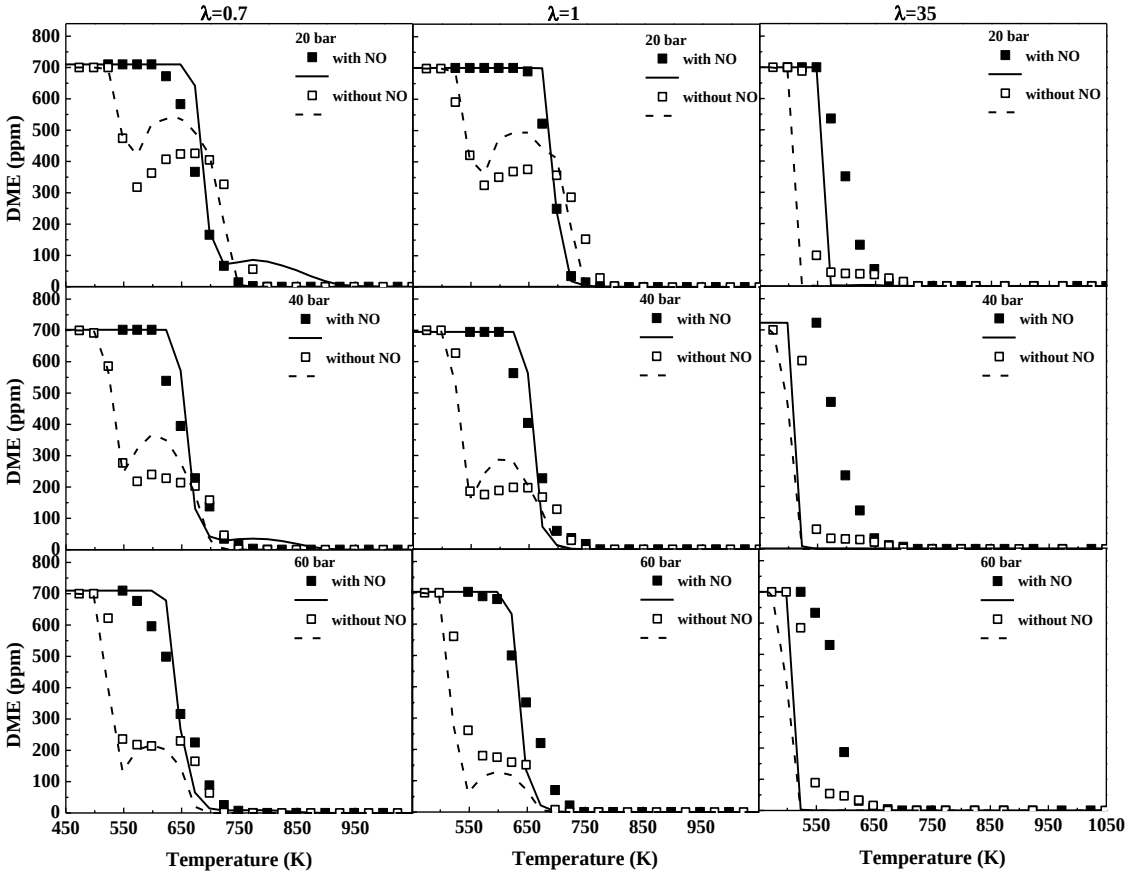

Figure 4. Evaluation of the effect of NO presence (500 ppm) on the high-pressure (20, 40 and 60 bar) oxidation of DME, for the conditions denoted as sets 1-9 and 13-21 in Table 1. Open symbols correspond to results in the absence of NO and full symbols, in the presence of NO.

In the absence of NO (denoted by open symbols), for the same value of lambda, as the pressure is increased, that is, to descend in a column in Figure 4, the consumption of DME occurs at lower temperatures and the NTC zone, instead of a curve, presents the shape of a plateau. For a constant value of pressure, an increase of the oxygen availability in the reactant mixture, that is, to move to the right in the same row of Figure 4, makes the NTC zone less pronounced. For oxidizing conditions (λ=35), it is less noticed because it occurs when the conversion of DME is near the 100%.

The inhibiting effect of NO addition is evident. The NTC zone disappears and the onset of DME conversion is shifted to higher temperatures for all the conditions analyzed in this work. However, due to the OH radicals generated during the NO_2 conversion to NO

($NO_2 + H \rightleftharpoons NO + OH$), NO can also promote DME conversion at higher temperatures above NTC zone, as can be observed, for example, at 20 bar, reducing conditions (λ=0.7) and temperatures around 775 K, and stoichiometric conditions (λ=1) and temperatures around 700 K. Once the DME conversion is initiated, its consumption occurs very fast, with a sharp decay in the DME concentration profile.

The inhibiting or promoting impact of NO on hydrocarbon oxidation has been previously discussed during the oxidation of alkanes that present the NTC zone, such as n-heptane in jet-stirred reactors [8, 13], or n-pentane in an atmospheric quartz flow reactor [9]. The previous work of Alzueta et al. [17] on the interaction of DME with NO, in an atmospheric flow reactor, pointed out the promoting effect of NO addition on DME conversion under oxidizing conditions. However, unlike the present work, in the atmospheric pressure study, the NTC zone was not observed and DME consumption occurred at much higher temperatures, above 1000 K in the absence of NO. Nevertheless, it is worth to mention that because of the different pressures analyzed in each study (atmospheric or high pressure) there is a huge difference in the residence time between the Alzueta et al.'s [17] and the present works, t_r(s)=190/T(K) and t_r (s)=261 P(bar)/T(K), respectively.

Regarding modeling calculations, under very oxidizing conditions (λ=35), the experimental trend observed for DME concentration in the presence of NO (Figure 4) is not accurately reproduced by the model. In this case, simulations are almost the same with and without NO, but experimental results obtained in the presence of NO are shifted to higher temperatures, approximately 25 K. As will be seen later in the sensitivity analysis, calculations indicate that the concentration profiles are sensitive to the isomerization of alkyl peroxyl radicals ($CH_3OCH_2O_2$=$CH_2OCH_2O_2H$). In order to evaluate the sensitivity of this reaction, Figure S18 in Supplementary Material shows the comparison between experimental and calculations using both the mechanism used along the present work and the same mechanism substituting the Burke et al. [29] determination by a non-pressure dependent value by Zhao et al. [28]. As seen, the fitting of experimental data and calculated results vary with the use of the non-dependent

rate constant, and it improves for λ=35. Therefore, we believe that a deeper study for this important reaction for the flow reactor experiments would be of interest. Despite of this, in general, there is a good agreement between experimental results and modeling calculations, both in the absence and presence of NO.

4.3 Reaction rate and first-order sensitivity analyses

Once the effectiveness of the present model has been proved, and in order to identify the main reaction routes for DME consumption, and especially, the routes responsible for NO inhibiting effect, reaction rate analyses have been performed. The DME oxidation chemistry at low-temperatures is more complex than at higher temperatures as pointed out previously by Rodriguez et al. [4] in a JSR experimental work, and Tomlin et al. [37] and Eskola et al. [38] in theoretical works. Therefore, Figure 5 shows a diagram with the main DME consumption routes in the absence of NO, for 600 K, a temperature included in the NTC zone.

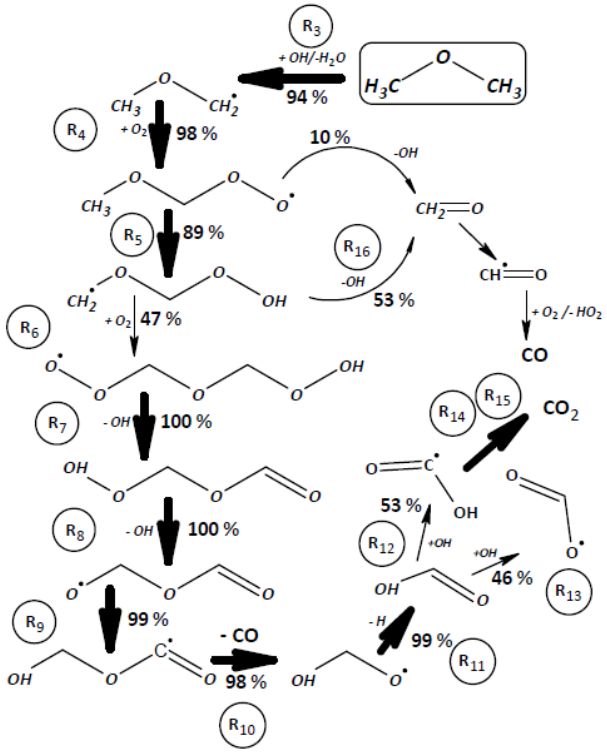

Figure 5. Main reaction pathways for DME oxidation at 600 K. Conditions denoted as set 2 in Table 1 (20 bar, λ=1, in the absence of NO). The selected position in the reactor corresponds to 57.4 cm, the point at which the temperature profile reaches the plateau.

The main consumption of DME is through hydrogen abstraction reactions by radicals to form the CH_3OCH_2 radical (R_3). This radical leads to the formation of methoxy methyl peroxy radical ($CH_3OCH_2O_2$) after the addition of a molecule of oxygen (R_4). The $CH_3OCH_2O_2$ radical leads to the formation of the hydroperoxyl-methylformate (HO_2CH_2OCHO) through a complex mechanism which involves an isomerization (R_5), a second O_2 addition (R_6) and a new isomerization followed by a decomposition (R_7).

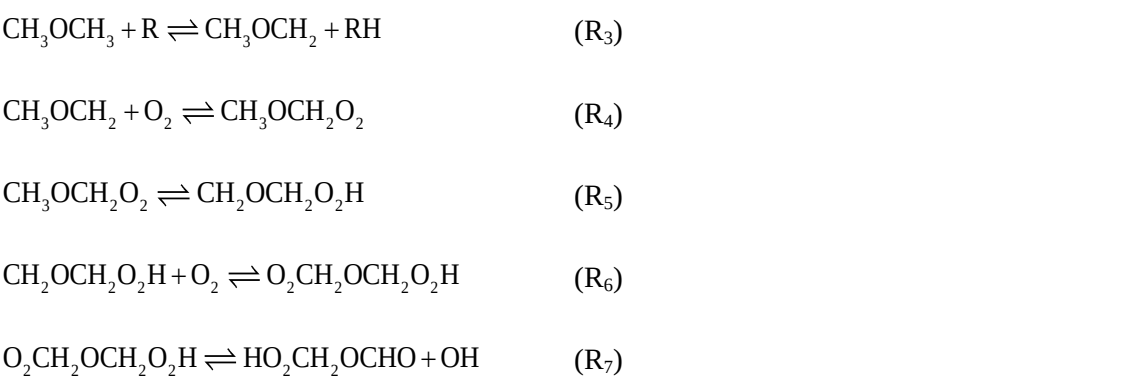

$$CH_3OCH_3 + R \rightleftharpoons CH_3OCH_2 + RH \quad (R_3)$$

$$CH_3OCH_2 + O_2 \rightleftharpoons CH_3OCH_2O_2 \quad (R_4)$$

$$CH_3OCH_2O_2 \rightleftharpoons CH_2OCH_2O_2H \quad (R_5)$$

$$CH_2OCH_2O_2H + O_2 \rightleftharpoons O_2CH_2OCH_2O_2H \quad (R_6)$$

$$O_2CH_2OCH_2O_2H \rightleftharpoons HO_2CH_2OCHO + OH \quad (R_7)$$

After subsequent isomerization and decomposition reactions formic acid is formed (sequence of reactions R_8-R_{11})

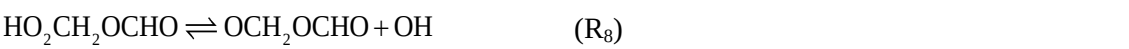

$$HO_2CH_2OCHO \rightleftharpoons OCH_2OCHO + OH \quad (R_8)$$

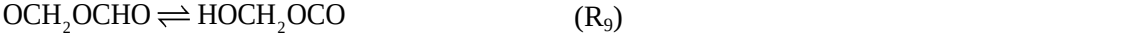

$$OCH_2OCHO \rightleftharpoons HOCH_2OCO \quad (R_9)$$

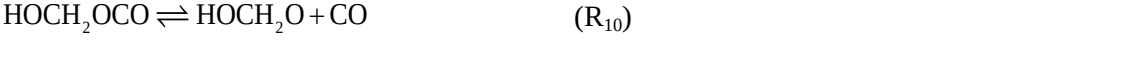

$$HOCH_2OCO \rightleftharpoons HOCH_2O + CO \quad (R_{10})$$

$$HOCH_2O \rightleftharpoons HCOOH + H \quad (R_{11})$$

and it continues reacting until CO_2 is produced (sequence of reactions R_{12}-R_{15}).

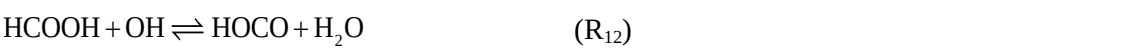

$$HCOOH + OH \rightleftharpoons HOCO + H_2O \quad (R_{12})$$

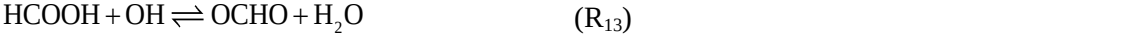

$$HCOOH + OH \rightleftharpoons OCHO + H_2O \quad (R_{13})$$

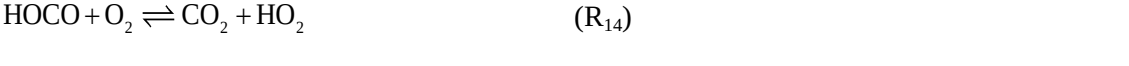

$$HOCO + O_2 \rightleftharpoons CO_2 + HO_2 \quad (R_{14})$$

$$OCHO \rightleftharpoons CO_2 + H \quad (R_{15})$$

During this complex reaction mechanism, hydroxyl radicals are released, which are responsible for the high reactivity of DME at low temperatures. As temperature increases, β-scission of the $CH_2OCH_2O_2H$ radical forming 2 molecules of formaldehyde and only one reactive hydroxyl

radical (R_{16}) becomes more relevant and, therefore, the DME reactivity decreases (NTC zone appears). For example, at 20 bar, in the absence of NO and λ=1, reaction (R_{16}) at 525 K represents a 6% of the $CH_2OCH_2O_2H$ radical total consumption, whereas at 600 K it represents a 53% and at 700 K, a 94%. Another β-scission reaction with increasing relevance with increasing temperature is the decomposition of CH_3OCH_2 radical forming formaldehyde and CH_3 radicals (R_{17}). Decomposition of CH_3OCH_2 radical (R_{17}) is almost negligible at 600 K, it represents a 20% of radical consumption at 700 K and a 53% at 750 K, under the same conditions above specified.

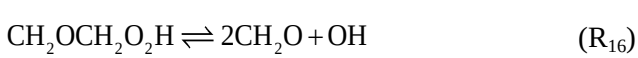

$$CH_2OCH_2O_2H \rightleftharpoons 2CH_2O + OH \qquad (R_{16})$$

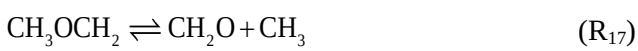

$$CH_3OCH_2 \rightleftharpoons CH_2O + CH_3 \qquad (R_{17})$$

Figure 6 shows the main reaction pathways for DME consumption at 700 K, in the presence of NO (500 ppm). As in the absence of NO, the main consumption for DME is through H abstraction reactions forming the CH_3OCH_2 radical (R_3). This radical can lead to the formation of $CH_3OCH_2O_2$ radical by the addition of an oxygen molecule (R_4) and continues the reaction mechanism described above in the absence of NO, although this pathway has a lower relevance. However, a new reaction route involving NO and NO_2 competes with this first addition of O_2. CH_3OCH_2 radical can react with NO_2 leading to the formation of NO and a new radical, CH_3OCH_2O (R_{18}). This radical, which can also be produced by reaction of $CH_3OCH_2O_2$ and NO (R_{19}), later decomposes to formaldehyde (R_{20}). Therefore, in addition to reaction (R_2), NO and NO_2 are interchanged through reactions (R_{18}-R_{19}), but never consumed.

$$CH_3OCH_2 + NO_2 \rightleftharpoons CH_3OCH_2O + NO \qquad (R_{18})$$

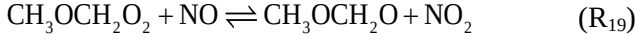

$$CH_3OCH_2O_2 + NO \rightleftharpoons CH_3OCH_2O + NO_2 \qquad (R_{19})$$

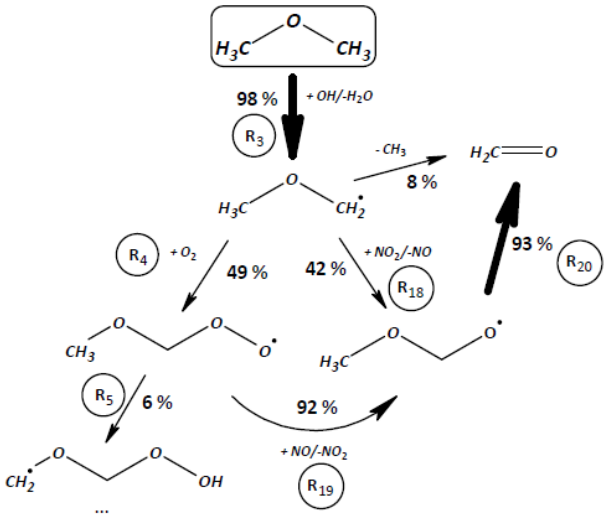

Figure 6. Main reaction pathways for DME oxidation at 700 K. Conditions denoted as set 14 in Table 1 (20 bar, λ=1, in the presence of NO). The selected position in the reactor corresponds to 57.4 cm, the point at which the temperature profile reaches the plateau.

In the decomposition of CH_3OCH_2O (R_{20}), besides formaldehyde, methoxy radicals (CH_3O) are also formed, and then react with O_2, NO_2 or NO to produce more formaldehyde (R_{21}-R_{23}). There is a competition between these three CH_3O consumption reactions, with reaction with O_2 (R_{21}) being the most relevant, followed by the reaction with NO_2 (R_{22}) and finally by the reaction with NO (R_{23}).

$$CH_3OCH_2O \rightleftharpoons CH_3O + CH_2O \qquad (R_{20})$$

$$CH_3O + O_2 \rightleftharpoons CH_2O + HO_2 \qquad (R_{21})$$

$$CH_3O + NO_2 \rightleftharpoons CH_2O + HONO \qquad (R_{22})$$

$$CH_3O + NO \rightleftharpoons CH_2O + HNO \qquad (R_{23})$$

The analysis of the reaction pathways has been completed with a first-order sensitivity analysis for CO for the different air excess ratios analyzed, 20 bar and in the absence and presence of NO. In each case, temperatures near the initiation of DME conversion, at which the CO concentration predicted by the model corresponds to a value around 30 ppm, have been selected.

Figure 7 shows a comparison of the sensitivity coefficients obtained in the presence and in the absence of NO.

In the absence of NO, the isomerization of the methoxy methyl peroxy radical ($CH_3OCH_2O_2$) (R_5) and the decomposition of the hydroperoxyl-methylformate (HO_2CH_2OCHO) (R_8) present a high sensitivity due to the OH radicals generated directly, in the decomposition, or indirectly through the low-temperature mechanism described previously and represented in Figure 5. This mechanism involves the $CH_3OCH_2O_2$ isomerization (R_5) and the O_2 addition to $CH_2OCH_2O_2H$ (R_6), also with a high sensitivity coefficient. In an opposite way, the self-reaction of $CH_3OCH_2O_2$ radicals results in less CO formation because it reduces the amount of $CH_3OCH_2O_2$ radicals than can react through the low-temperature mechanism.

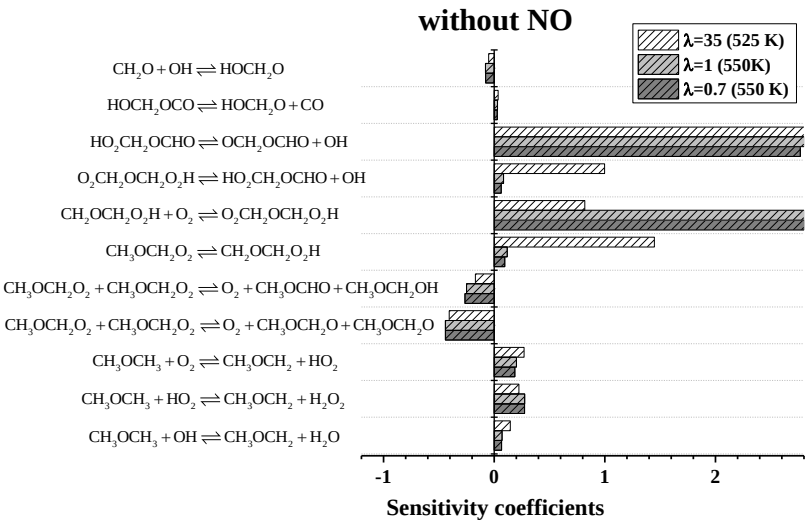

408

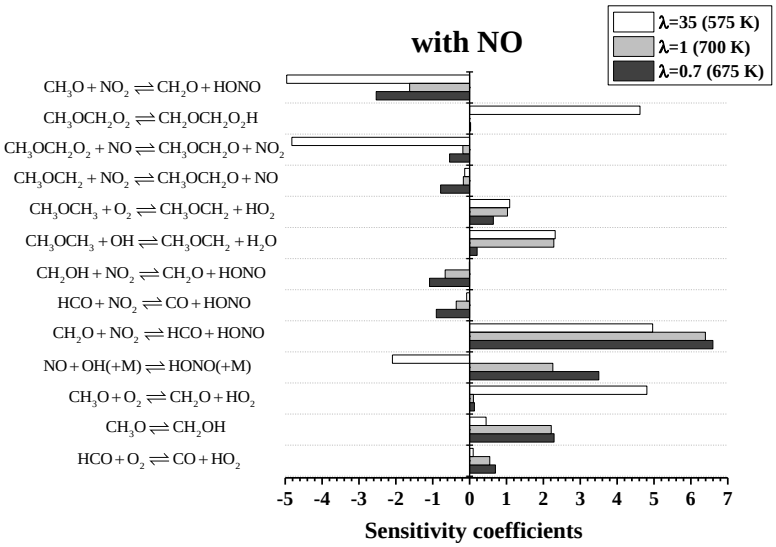

409

Figure 7. Sensitivity analysis for CO for different air excess ratios and 20 bar. Top: in the absence of NO. Bottom: in the presence of NO.

In the presence of NO, the reaction of $CH_3OCH_2O_2$ with NO (generally represented as RO_2+NO=RO+NO_2, R_{19}) decreases the global system reactivity. This reaction, that is in competition with reaction (R_5), reduces the availability of hydroperoxide species (RO_2) and, therefore, the formation of hydroxyl radicals from hydroperoxide decomposition reactions during the low-temperature mechanism, because the resulting RO radical decomposes directly to formaldehyde (R_{20}). On the contrary, the isomerization of $CH_3OCH_2O_2$ has a positive sensitivity coefficient (R_5), because, as in the absence of NO, this reaction corresponds to the initial steps of the low-temperature mechanism.

5. Conclusions

The effect of NO presence on the DME high pressure oxidation has been evaluated by means of novel experimental results obtained in a plug flow reactor at 20, 40 and 60 bar, in the 450-1050 K range and for different values of the air excess ratio (λ=0.7, 1 and 35). Additionally, a chemical kinetic mechanism has been used which provides a good agreement with the trends experimentally observed. Moreover, modeling calculations with the present mechanism have been successfully compared with experimental data from literature.

The presence of NO clearly inhibits DME oxidation in the 550-700 K temperature range, where the NTC zone was previously observed in the absence of NO. Reaction rate analyses performed indicate that the main consumption of DME is through H abstraction forming the CH_3OCH_2 radical ($CH_3OCH_3 + R \rightleftharpoons CH_3OCH_2 + RH$). In the absence of NO, it reacts with O_2 to form $CH_3OCH_2O_2$ ($CH_3OCH_2 + O_2 \rightleftharpoons CH_3OCH_2O_2$) and it continues reacting through a complex mechanism while OH radicals are generated. But, in the presence of NO, the CH_3OCH_2+O_2 reaction is in competition with CH_3OCH_2+NO_2 channel producing NO which reacts with $CH_3OCH_2O_2$ ($CH_3OCH_2O_2 + NO \rightleftharpoons CH_3OCH_2O + NO_2$), inhibiting the low-temperature DME oxidation. Consequently, NO and NO_2 are interchanged in a cycle but never consumed.

Acknowledgements

The authors express their gratitude to Aragón Government and European Social Fund (GPT group), and to MINECO and FEDER (Project CTQ2015-65226) for financial support. Ms. Marrodán acknowledges Aragón Government for the predoctoral grant awarded.

References

[1] C. Arcoumanis, C. Bae, R. Crookes, E. Kinoshita, The potential of di-methyl ether (DME) as an alternative fuel for compression-ignition engines: a review, Fuel 87 (2008) 1014-1030.

[2] S.H. Park, C.S. Lee, Combustion performance and emission reduction characteristics of automotive DME engine system, Prog. Energy Combust. Sci. 39 (2013) 147-168.

[3] T.A. Semelsberger, R.L Borup, H.L. J. Greene, Dimethyl ether (DME) as an alternative fuel, J. Power Sources 156 (2006) 497-511.

[4] A. Rodriguez, O. Frottier, O. Herbinet, R. Fournet, R. Bounaceur, C. Fittschen, F. Battin-Leclerc, Experimental and modeling investigation of the low-temperature oxidation of dimethyl ether, J. Phys. Chem. A 119 (2015) 7905-7923.

[5] U. Asad, M. Zheng, Exhaust gas recirculation for advanced diesel combustion cycles, Appl. Energy 123 (2014) 242-252.

[6] J.E. Dec, Advanced compression-ignition engines. Understanding the in-cylinder processes, Proc. Combust. Inst. 32 (2009) 2727-2742.

[7] Z. Chen, P. Zhang, Y. Yang, M.J. Brear, X. He, Z. Wang, Impact on nitric oxide (NO) on n-heptane autoignition in a rapid compression machine, Combust. Flame 186 (2017) 94-104.

[8] G. Moréac, P. Dagaut, J.F. Roesler, M. Cathonnet, Nitric oxide interactions with hydrocarbon oxidation in a jet-stirred reactor at 10 atm, Combust. Flame 145 (2006) 512-520.

[9] P.A. Glaude, N. Marinov, Y. Koshiishi, N. Matsunaga, M. Hori, Kinetic modeling of the mutual oxidation of NO and larger alkanes at low temperature, Energy Fuels 19 (2005) 1839-1849.

[10] P. Dagaut, A. Nicolle, Experimental study and detailed kinetic modeling of the effect of exhaust gas on fuel combustion: mutual sensitization of the oxidation of nitric oxide and methane over extended temperature and pressure ranges, Combust. Flame 140 (2005) 161-171.

[11] P. Dagaut, J. Luche, M. Cathonnet, Reduction of NO by n-butane in a JSR: experiments and kinetic modeling, Energy Fuels 14 (2000) 712-719.

[12] A.B. Bendtsen, P. Glarborg, K. Dam-Johansen, Low temperature oxidation of methane: the influence of nitrogen oxides, Combust. Sci. Technol. 151 (2000) 31-71.

[13] J.M. Anderlohr, R. Bounaceur, A. Pires Da Cruz, F. Battin-Leclerc, Modeling of autoignition and NO sensitization for the oxidation of IC engine surrogate fuels, Combust. Flame 156 (2009) 505-521.

[14] M.U. Alzueta, J.M. Hernández, Ethanol oxidation and its interaction with nitric oxide, Energy Fuels 16 (2002) 166-171.

[15] M.U. Alzueta, R. Bilbao, M. Finestra, Methanol oxidation and its interaction with nitric oxide, Energy Fuels 15 (2001) 724-729.

[16] P. Glarborg, M.U Alzueta, K. Dam-Johansen, J.A. Miller, Kinetic modeling of hydrocarbon/nitric oxide interactions in a flow reactor, Combust. Flame 115 (1998) 1-27.

[17] M.U. Alzueta, J. Muro, R. Bilbao, P. Glarborg, Oxidation of dimethyl ether and its interaction with nitrogen oxides, Isr. J. Chem. 39 (1999) 73-86.

[18] L. Marrodán, L. Berdusán, V. Aranda, Á. Millera, R. Bilbao, M.U. Alzueta, Influence of dimethyl ether addition on the oxidation of acetylene in the absence and presence of NO, Fuel 183 (2016) 1-8.

[19] L. Marrodán, Á. Millera, R. Bilbao, M.U. Alzueta, High-pressure study of methyl formate oxidation and its interaction with NO, Energy Fuels 28 (2014) 6107-6115.

[20] C.L. Rasmussen, J. Hansen, P. Marshall, P. Glarborg, Experimental measurements and kinetic modeling of $CO/H_2/O_2/NO_x$ conversion at high pressure, Int. J. Chem. Kinet. 40 (2008) 454-480.

[21] P. Glarborg, M. Østberg, M.U. Alzueta, K. Dam-Johansen, J.A. Miller, The recombination of hydrogen atoms with nitric oxide at high temperatures, Proc. Combust. Inst. 27 (1999) 219-227.

[22] M.U. Alzueta, M. Borruey, A. Callejas, Á. Millera, R. Bilbao, An experimental and modeling study of the oxidation of acetylene in a flow reactor, Combust. Flame 152 (2008) 377-386.

[23] N. Faßheber, G. Friedrichs, P. Marshall, P. Glarborg, Glyoxal oxidation mechanism: implications for the reactions $HCO+O_2$ and $OCHCHO+HO_2$, J. Phys. Chem. A 119 (2015) 7305-7315.

[24] C.L. Rasmussen, P. Glarborg, Measurements and kinetic modeling of CH_4/O_2 and $CH_4/C_2H_6/O_2$ conversion at high-pressure, Int. J. Chem. Kinet. 40 (2008) 778-807.

[25] C.L. Rasmussen, K.H. Andersen, K. Dam-Johansen, P. Glarborg, Methanol oxidation in a flow reactor: implications for the branching ratio of the CH_3OH+OH reaction, Int. J. Chem. Kinet. 40 (2008) 423-441.

[26] C.L. Rasmussen, P. Glarborg, Sensitizing effects of NO_x on CH_4 oxidation at high pressure, Combust. Flame 154 (2008) 529-545.

[27] J. Giménez-López, C.T. Rasmussen, H. Hashemi, M.U. Alzueta, Y. Gao, P. Marshall, C.F. Goldsmith, P. Glarborg, Experimental and kinetic modeling study of C_2H_2 oxidation at high pressure, Int. J. Chem. Kinet. 48 (2016) 724-738.

[28] Z. Zhao, M. Chaos, A. Kazakov, F.L. Dryer, Thermal decomposition reaction and a comprehensive kinetic model of dimethyl ether, Int. J. Chem. Kinet. 40 (2008) 1-18.

[29] U. Burke, K.P. Somers, P. O'Toole, C.M. Zinner, N. Marquet, G. Bourque, E.L. Petersen, W.K. Metcalfe, Z. Serinyel, H.J. Curran, An ignition delay and kinetic modeling study of methane, dimethyl ether, and their mixtures at high pressures, Combust. Flame 162 (2015) 315-330.

[30] Z. Wang, X. Zhang, L. Xing, L. Zhang, F. Herrmann, K. Moshammer, F. Qi, K. Kohse-Höinghaus, Combust. Flame 162 (2015) 1113-1125.

[31] E.E. Dames, A.S. Rosen, B.W. Weber, C.W. Gao, C-J. Sung, W.H. Green, A detailed combined experimental and theoretical study on dimethyl ether/propane blended oxidation, Combust. Flame 168 (2016) 310-330.

[32] P. Marshall, P. Glarborg, Ab initio and kinetic modeling studies of formic acid oxidation, Proc. Combust. Inst. 35 (2015) 153-160.

[33] L. Marrodán, E. Royo, Á. Millera, R. Bilbao, M.U. Alzueta, High pressure oxidation of dimethoxymethane, Energy Fuels 29 (2015) 3507-3517.

[34] L. Marrodán, Á.J. Arnal, Á. Millera, R. Bilbao, M.U. Alzueta, High-pressure ethanol oxidation and its interaction with NO, Fuel 223 (2018) 394-400.

[35] T. Yamada, J.W. Bozelli, T.H. Lay, Comparisons of CBS-q and G2 calculations on thermodynamic properties, transition states, and kinetics on dimethyl-ether+O_2 reaction system, Int. J. Chem. Kinet. 32 (2000) 435-452.

[36] ANSYS Chemkin-Pro 17.2; Reaction Design: San Diego, 2016.

[37] A.S. Tomlin, E. Agbro, V. Nevrlý, J. Dlabka, M. Vašinek, Evaluation of combustion mechanisms using global uncertainty and sensitivity analyses: a case study for low-temperature dimethyl ether oxidation, Int. J. Chem. Kinet. 46 (2014) 662-682.

[38] A.J. Eskola, S.A. Carr, R.J. Shannon, B. Wang, M.A. Blitz, M.J. Pilling, P.W. Seakins, S.H. Robertson, Analysis of the kinetics and yields of OH radical production from the CH_3OCH_2+O_2 reaction in the temperature range 195-650 K: an experimental and computational study, J. Phys. Chem. A 118 (2014) 6773-6788.